Spatial Structures of Anomalously Localized States in Tail Regions at the Anderson Transition

H. Obuse and K. Yakubo

Department of Applied Physics, Graduate School of Engineering, Hokkaido University, Sapporo 060-8628, Japan.

We study spatial structures of anomalously localized states (ALS) in tail regions at the critical point of the Anderson transition in the two-dimensional symplectic class. In order to examine tail structures of ALS, we apply the multifractal analysis only for the tail region of ALS and compare with the whole structure. It is found that the amplitude distribution in the tail region of ALS is multifractal and values of exponents characterizing multifractality are the same with those for typical multifractal wavefunctions in this universality class.

KEYWORDS: Anderson transition, critical states, multifractal, anomalously localized states, two-dimensional symplectic system

1. Introduction

Disorder induced metal-insulator transition at absolute zero temperature, namely, the Anderson transition, has been extensively studied since the seminal paper by Anderson.[1] Although the vast amount of knowledge on this physical phenomenon has been accumulated for half a century, there still exist fundamental problems on properties of non-interacting electrons in disordered systems. One of such unsettled questions is anomalously localized states (ALS)[2,3] in which most of amplitudes concentrate on a narrow spatial region even in a metallic phase. The existence of ALS was analytically predicted, and the nature of ALS has been numerically and analytically studied.[4–17] Most of previous works on ALS focused on the amplitude distribution function, which mainly reflects peak structures of ALS. Falko *et al.*[5] and Uski *et al.*[11] have predicted that the spatial correlation function of amplitudes has a long tail. This implies that ALS are not truely localized. The tail structure of ALS is crucial for understanding transport properties of metals.

Recently, we have shown that ALS also exist at the critical point of the Anderson transition with a finite probability even in infinite systems.[18–20] It is well known that wavefunctions at metal-insulator transition point show multifractality reflecting the absence of characteristic lengths in critical wavefunctions.[21–23] Because of a confining length of ALS, ALS wavefunctions are not, however, multifractal. The finite probability of ALS implies that ALS contradict well known critical properties such as universality, the scaling concept, and the idea of renormalization. Our results suggest that these critical properties should be considered for typical critical states. It is natural to suppose that the critical level statistics is also influenced by ALS. Our previous works, however, show that ALS do not contribute to the level statistics.[20] To understand this fact, it is quite important to reveal the tail structure of ALS wavefunctions.

In this paper, we investigate spatial structures of ALS wavefunctions at the critical point of the Anderson transition in the two-dimensional symplectic class. It is found that the amplitude distribution of ALS in their tail region actually shows multifractality and values of exponents characterizing multifractality are the same with those for typical multifractal wavefunctions for this universality class. This paper is organized as follows. In §2, we give a quantitative definition of ALS at the critical point based on the idea that ALS at criticality do not show multifractality. In §3, the basic multifractal analysis is remained. We briefly explain, in §4, the employed SU(2) model which belongs to the symplectic class and a numerical method to obtain eigenstates of systems described by this model. Numerical results and conclusions are given in §5.

2. Definition of Anomalously Localized States

In order to study ALS, we employ a definition of ALS proposed in ref. 18. This definition is based on the idea that ALS are not multifractal as a consequence of their localized nature. At first, we introduce the box-measure correlation function $G_q(l,L,r)$ defined by[24,25]

$$G_q(l,L,r) = \frac{1}{N_b N_{b_r}} \sum_b \sum_{b_r} \mu^q_{b(l)} \mu^q_{b_r(l)}, \tag{1}$$

where $\mu_{b(l)} = \sum_{i\in b(l)} |\psi_i|^2$ and $\mu_{b_r(l)} = \sum_{i\in b_r(l)} |\psi_i|^2$ are box measures for wavefunction amplitudes ψ_i, in a box $b(l)$ of size l and in a box $b_r(l)$ of size l fixed distance $r-l$ away from the box $b(l)$, respectively. N_b (or N_{b_r}) is the number of boxes $b(l)$ [or $b_r(l)$], and the summation $\sum_b$ (or $\sum_{b_r}$) is taken over all boxes $b(l)$ [or $b_r(l)$] in the system of size L. If a wavefunction is multifractal, $G_q(l,L,r)$ should behave as[25]

$$G_q(l,L,r) \propto l^{x(q)} L^{-y(q)} r^{-z(q)}, \tag{2}$$

where $x(q)$, $y(q)$, and $z(q)$ are exponents describing multifractal correlations of the amplitude distribution. This relation is sensitive to ALS as demonstrated in ref. 18 and then suitable for defining ALS. To find the l and r dependences of $G_q(l,L,r)$, we concentrate on the following functions,

$$Q_q(l) = G_q(l,L,r=l) \propto l^{x(q)-z(q)}, \tag{3}$$

and

$$R_q(r) = G_q(l=1,L,r) \propto r^{-z(q)}. \tag{4}$$

In order to quantify non-multifractality of a specific wavefunction, it is convenient to introduce variances $\mathrm{Var}(\log Q_2)$ and $\mathrm{Var}(\log R_2)$ from the linear functions of $\log l$ and $\log r$, $\log Q_2(l) = [x(2) - z(2)]\log l + c_Q$ and $\log R_2(r) = -z(2)\log r + c_R$, respectively, calculated by the least-square fit. From these variances, we define a quantity Γ as

$$\Gamma = \lambda \mathrm{Var}(\log Q_2) + \mathrm{Var}(\log R_2), \tag{5}$$

where λ is a factor to compensate the difference between average values of $\mathrm{Var}(\log Q_2)$ and $\mathrm{Var}(\log R_2)$. Using Γ given by eq. (5), the quantitative and expediential definition of ALS at criticality is presented by

$$\Gamma > \Gamma^*, \tag{6}$$

where Γ^* is a criterial value of Γ to distinguish ALS from multifractal states.

3. Multifractal Analysis

In this section, we give some definitions of basic quantities and exponents used in the multifractal analysis. At first, we introduce a quantity $Z(q)$ defined by

$$Z_q(l) = \sum_b \mu_{b(l)}^q. \tag{7}$$

Here, symbols and notations in eq. (7) have the same meanings of those in eq. (1). For a multifractal wavefunction, $Z_q(l)$ obeys a power law

$$Z_q(l) \propto l^{\tau(q)}, \tag{8}$$

where $\tau(q)$ is called the mass exponent. From eq. (8), the mass exponent is given by

$$\tau(q) = \lim_{l\to 0} \frac{\log Z_q(l)}{\log l}. \tag{9}$$

Using $\tau(q)$, the generalized dimension D_q is defined as

$$D_q = \frac{\tau(q)}{q-1}, \tag{10}$$

particulary, D_q for $q = 2$ (thus D_2) is called the correlation dimension.

The multifractal spectrum $f(\alpha)$ is defined by the Legendre transform of $\tau(q)$, i.e., $f(\alpha) = \alpha q - \tau(q)$, where the Lipschitz-Hölder exponent α is defined by $\alpha = d\tau(q)/dq$. The multifractal spectrum $f(\alpha)$ has the meaning of the fractal dimension of the spatial distribution of boxes characterized by the exponent α. The multifractal spectrum $f(\alpha)$ and the Lipschitz-Hölder α can be also calculated directly from box measures of wavefunction amplitudes as[30]

$$f(\alpha) = \lim_{l\to 0} \frac{\sum_b m_{b(l)}(q)\log m_{b(l)}(q)}{\log l}, \tag{11}$$

and

$$\alpha = \lim_{l\to 0} \frac{\sum_b m_{b(l)}(q)\log \mu_{b(l)}}{\log l}, \tag{12}$$

respectively. Here, $m_{b(l)}(q)$ called the q-microscope is defined by

$$m_{b(l)}(q) = \frac{\mu_{b(l)}^q}{\sum_{b'} \mu_{b'(l)}^q}. \tag{13}$$

4. System and Numerical Method

Considering the advantage of system sizes, we focus our attention on the Anderson transition in two-dimensional electron systems with strong spin-orbit interactions, in which systems have no spin-rotational symmetry but have the time-reversal one. Hamiltonians describing these systems belong to the symplectic class. Among several models belonging to this universality class, we adopt the SU(2) model because of its small scaling corrections. The Hamiltonian of the SU(2) model[26] is given by

$$\boldsymbol{H} = \sum_i \varepsilon_i \boldsymbol{c}_i^\dagger \boldsymbol{c}_i - V \sum_{i,j} \boldsymbol{R}_{ij} \boldsymbol{c}_i^\dagger \boldsymbol{c}_j, \tag{14}$$

where $\boldsymbol{c}_i^\dagger$ ($\boldsymbol{c}_i$) is the creation (annihilation) operator acting on a quaternion state vector, $\boldsymbol{R}_{ij}$ is the quaternion-real hopping matrix element between the sites i and j, and ε_i denotes the on-site random potential distributed uniformly in the interval $[-W/2, W/2]$. (Bold symbols represent quaternion-real quantities.) The matrix element $\boldsymbol{R}_{ij}$ is given by

$$\begin{aligned} \boldsymbol{R}_{ij} &= \cos\alpha_{ij}\cos\beta_{ij}\boldsymbol{\tau}^0 + \sin\gamma_{ij}\sin\beta_{ij}\boldsymbol{\tau}^1 \\ &- \cos\gamma_{ij}\sin\beta_{ij}\boldsymbol{\tau}^2 + \sin\alpha_{ij}\cos\beta_{ij}\boldsymbol{\tau}^3, \end{aligned} \tag{15}$$

for the nearest neighbor sites i and j, and $\boldsymbol{R}_{ij} = 0$ for otherwise. Here, $\boldsymbol{\tau}^\mu$ ($\mu = 0, 1, 2, 3$) is the primitive element of quaternions.[27] Random quantities α_{ij} and γ_{ij} are distributed uniformly in the range of $[0, 2\pi)$, and β_{ij} is distributed according to the probability density $P(\beta)d\beta = \sin(2\beta)d\beta$ for $0 \le \beta \le \pi/2$. Randomly distributed hopping matrix elements shorten the spin relaxation length which is a dominant irrelevant length scale. Thus, scaling corrections become very small in the SU(2) model. It is known that the localization length exponent ν of this model is 2.73 ± 0.02 and the critical disorder W_c is $5.952V$ at $E = 1.0V$.[26]

Critical wavefunctions of the SU(2) model have been calculated by using the forced oscillator method (FOM)[28] extended to eigenvalue problems of quaternion-real matrices. Of course, the Hamiltonian eq. (14) can be represented by complex numbers, and we can use the usual FOM for complex Hermitian matrices to solve the eigenvalue problem. The modified FOM for quaternion-real matrices, however, enables us to calculate eigenvalues and eigenvectors within about a half of CPU time.[29] It should be remarked that the obtained eigenvector is a quaternion-real vector. This vector represents two physical states simultaneously, which correspond to the Kramers doublet. Since the amplitude distribution of these degenerate states are the same, we analyze one of the calculated Kramers doublet.

5. Results and Conclusions

In this section, we show the results of the multifractal analysis for amplitude distribution of ALS in the tail region. At first, we look for ALS according to our definition of eq. (6). In this work, the criterial value is $\Gamma^* = 0.03$. For this purpose, we calculate 10^4 critical wavefunctions for the SU(2) model at $E = 1.0V$ and $W = 5.952V$ by means of the FOM. Each eigenstate is obtained for a

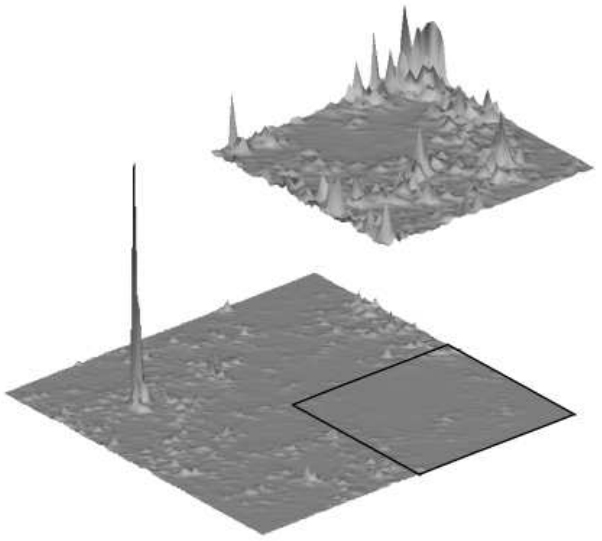

Fig. 1. Squared amplitudes of a wavefunction $\psi_{\rm ALS}$ for the SU(2) model of the system size $L = 120$ (lower figure). The value characterizing non-multifractality defined by eq. (5) is $\Gamma = 0.10$. The square enclosed by solid lines represents a tail region. The upper figure shows squared amplitudes of the wavefunction $\psi_{\rm tail}$ of this tail region (the subsystem size is $L = 60$).

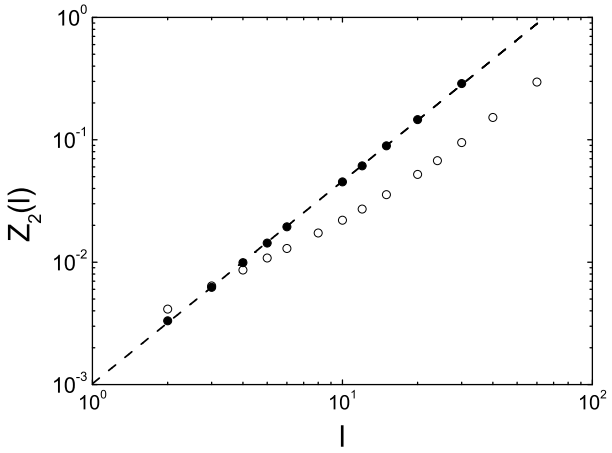

Fig. 2. $Z_2(l)$ for $\psi_{\rm ALS}$ (open circles) and $\psi_{\rm tail}$ (filled circles). The dashed line shows the least square fit for $Z_2(l)$ for $\psi_{\rm tail}$.

single disorder realization. Periodic boundary conditions are imposed in the x and y directions in the system of size $L = 120$.

Figure 1 shows squared amplitudes of a ALS wavefunction $\psi_{\rm ALS}$. The value of Γ of this wavefunction is $\Gamma = 0.10$. In this wavefunction, amplitudes concentrate in a narrow spatial region. The wavefunction appears to be localized for this feature. In order to investigate the tail structure of this wavefunction, we extract a part of the wavefunction within a 60×60 subsystem where the cut region is depicted in Fig. 1 by solid lines. The upper figure of Fig. 1 shows the extracted tail region wavefunction $\psi_{\rm tail}$. The amplitude distribution of $\psi_{\rm tail}$ is very complicated, and seems to be multifractal. To clarify this point, we examine below multifractality of $\psi_{\rm tail}$.

At first, we calculate $Z_2(l)$ given by eq. (7) for $\psi_{\rm ALS}$ and $\psi_{\rm tail}$. The wavefunction $\psi_{\rm tail}$ is normalized in the subsystem to perform the multifractal analysis. We see that $Z_2(l)$ for $\psi_{\rm ALS}$ does not exhibit the power law as shown in Fig. 2 (open circles). If ALS are truly localized such as $\psi_{\rm ALS}(r) \propto \exp(-r/\xi)$, where ξ is a localization length, $Z_2(l)$ for $\psi_{\rm ALS}$ should take a constant value for $l \gg \xi$. However, $Z_2(l)$ for ALS is not constant even for large l as shown in Fig. 2. On the contrary, the quantity $Z_2(l)$ for $\psi_{\rm tail}$ clearly obeys a power law as shown by filled circles in Fig. 2. The value of the correlation dimension $D_2 = \tau(2) = 1.69 \pm 0.01$ is very close to the value reported so far for typical multifractal wavefunctions belonging to this universality class.[18] This implies that tail regions of ALS exhibit the same multifractality with that of typical critical wavefunctions. The fact that the behavior of $Z_2(l)$ for $\psi_{\rm ALS}$ for $l \gg 20$ is similar to that for $\psi_{\rm tail}$ shows that $Z_2(l)$ at large l values is dominated by the tail structure of the ALS wavefunction.

Next, we calculate the multifractal spectra for both wavefunctions $\psi_{\rm ALS}$ and $\psi_{\rm tail}$. Results are shown in Fig. 3. Remarkably, $f(\alpha)$ for $\psi_{\rm ALS}$ takes negative values for small α, which is not reasonable because $f(\alpha)$ is the fractal dimension of the distribution of boxes characterized by α. This supports that $\psi_{\rm ALS}$ does not have a multifractal structure. On the other hand, $f(\alpha)$ for $\psi_{\rm tail}$ satisfies several conditions for multifractal spectra. The value of α_0 giving the maximum of $f(\alpha)$ for $\psi_{\rm tail}$ is $\alpha_0 = 2.15 \pm 0.02$, and the minimum and maximum values of α are estimated as $\alpha_{\rm min} = 1.22$ and $\alpha_{\rm max} = 3.26$, respectively. These values are very close to those for typical multifractal wavefunctions. In fact, we calculate $f(\alpha)$ for a typical critical wavefunction with $\Gamma = 0.001$ which is the smallest value of Γ in all calculated wavefunctions. Obtained values are $\alpha_0 = 2.17$, $\alpha_{\rm min} = 1.22$, and $\alpha_{\rm max} = 3.31$. The characteristic values of α for $\psi_{\rm tail}$ are also close to averaged values for an ensemble of typical critical wavefunctions.[19] The profile of $f(\alpha)$ for $\psi_{\rm tail}$ in the vicinity of $\alpha = \alpha_0$ can be well approximated by the

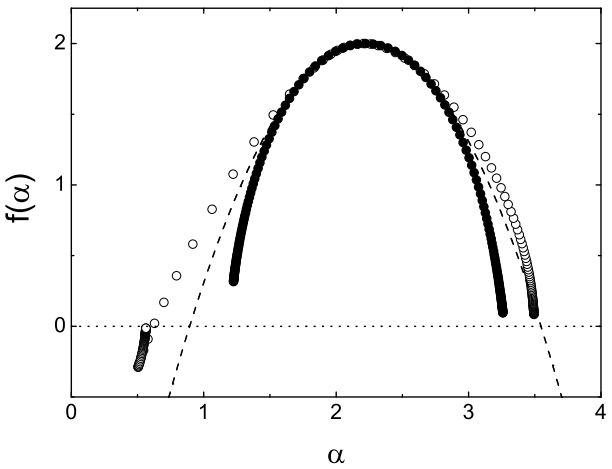

Fig. 3. Multifractal spectra $f(\alpha)$ for $\psi_{\rm ALS}$ (open circles) and $\psi_{\rm tail}$ (filled circles). The dashed line shows the parabolic approximation eq. (16) with $\alpha_0 = 2.15$.

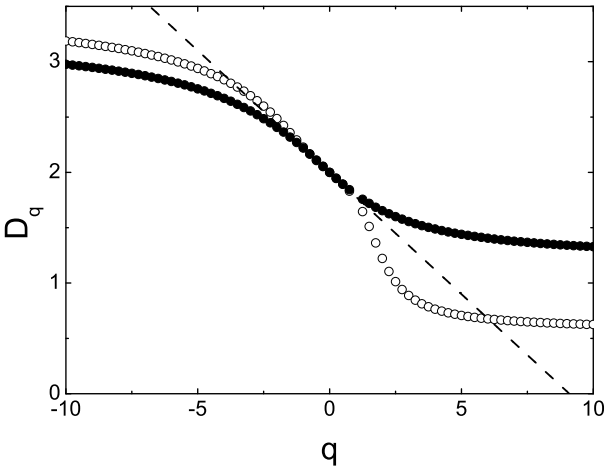

Fig. 4. The generalized dimension as a function of the moment q for $\psi_{\rm ALS}$ (open circles) and $\psi_{\rm tail}$ (filled circles). The dashed line represents the parabolic approximation eq. (17) with $\alpha_0 = 2.15$.

parabolic form

$$f(\alpha) = 2 - \frac{(\alpha_0 - \alpha)^2}{4(\alpha_0 - 2)}, \tag{16}$$

which is shown by dashed line in Fig. 3. These results ensure that $\psi_{\rm tail}$ has the same multifractal amplitude distribution with that for typical critical wavefunctions. It seems that $f(\alpha)$ for $\psi_{\rm ALS}$ is also fitted by eq. (16). This possibility is, however, denied when examining the generalized dimension D_q.

Figure 4 shows the generalized dimension D_q calculated by the box-counting method eq. (7) for both wavefunctions $\psi_{\rm ALS}$ and $\psi_{\rm tail}$. The values of D_q for two wavefunctions largely deviate each other for $|q| \gg 1$. Since $D_{-\infty}$ and D_{∞} are equal to $\alpha_{\rm max}$ and $\alpha_{\rm min}$, respectively, such large deviations are consistent with Fig. 3. The parabolic approximation of D_q corresponding to eq. (16) is given by

$$D_q = 2 - q(\alpha_0 - 2), \tag{17}$$

which would be valid in the vicinity of $q = 0$. The generalized dimension D_q for $\psi_{\rm tail}$ is well approximated by eq. (17) with $\alpha_0 = 2.15$ as shown by dashed line in Fig. 4. On the contrary, D_q for $\psi_{\rm ALS}$ does not follow a straight line near $q = 0$. This implies that the parabolic approximation eq. (16) does not reproduce $f(\alpha)$ for $\psi_{\rm ALS}$ even in the vicinity of $\alpha = \alpha_0$.

In summary, we investigate the spatial structure of ALS at the critical point of the Anderson transition. It is found that ALS are not truly localized and the tail structure of ALS shows the same multifractality with that of typical wavefunctions. These results form the foundation of understanding the distribution of physical quantities at criticality.

Acknowledgements

We are grateful to T. Nakayama for helpful discussions. This work was supported in part by a Grant-in-Aid for Scientific Research from Japan Society for the Promotion of Science (No. 14540317) and for the 21st Century Centre of Excellence (COE) Program, entitled "Topological Science and Technology", from the Ministry of Education, Culture, Sport, Science and Technology of Japan (MECSST). Numerical calculations in this work have been mainly performed on the facilities of the Supercomputer Center, Institute for Solid State Physics, University of Tokyo.

1) P. W. Anderson: Phys. Rev. **109** (1958) 1492.
2) B. L. Altshuler, V. E. Kravtsov, and I. V. Lerner: Pis'ma Zh. Eksp. Teor. Fiz. **45** (1987) 160 [JETP Lett. **45** (1987) 199].
3) For a comprehensive review, see A. D. Mirlin: Phys. Rep. **326** (2000) 259.
4) B. A. Muzykantskii and D. E. Khmelnitskii: Phys. Rev. B **51** (1995) 5480.
5) V. I. Falko and K. B. Efetov: Phys. Rev. B **52** (1995) 17413.
6) I. E. Smolyarenko and B. L. Altshuler: Phys. Rev. B **55** (1997) 10451.
7) I. Kogan, C. Mudry, and A. M. Tsvelik: Phys. Rev. Lett. **77** (1996) 707.
8) V. Uski, B. Mehlig, R. A. Römer, and M. Schreiber: Phys. Rev. B **62** (2000) R7699.
9) B. K. Nikolić: Phys. Rev. B **64** (2001) 14203.
10) B. K. Nikolić: Phys. Rev. B **65** (2002) 012201.
11) V. Uski, B. Mehlig, and M. Schreiber: Phys. Rev. B **66** (2002) 233104.
12) B. K. Nikolić and V. Z. Cerovski: Eur. Phys. J. B **30** (2002) 227.
13) V. M. Apalkov, M. E. Raikh, and B. Shapiro: Phys. Rev. Lett. **89** (2002) 16802.
14) V. M. Apalkov, M. E. Raikh, and B. Shapiro: Phys. Rev. Lett. **89** (2002) 126601.
15) T. Kottos, A. Ossipov, and T. Geisel: Phys. Rev. E **68** (2003) 066215.
16) A. Ossipov, T. Kottos, and T. Geisel: Europhys. Lett. **62** (2003) 719.
17) V. M. Apalkov, M. E. Raikh, and B. Shapiro: Phys. Rev. Lett. **92** (2004) 066601.
18) H. Obuse and K. Yakubo: Phys. Rev. B **69** (2004) 125301.
19) H. Obuse and K. Yakubo: J. Phys. Soc. Jpn. **73** (2004) 2164.
20) H. Obuse and K. Yakubo: Phys. Rev. B (to be published); cond-mat/0405429.
21) H. Aoki: J. Phys. C **16** (1983) L205; Phys. Rev. B **33** (1986) 7310.
22) F. Wegner: Z. Phys. B **36** (1980) 209.
23) T. Nakayama and K. Yakubo: *Fractal Concepts in Condensed Matter Physics.* (Springer-Verlag, Berlin, 2003).
24) M. E. Cates and J. M. Deutsch: Phys. Rev. A **35** (1987) 4907.
25) M. Janssen: Int. J. Mod. Phys. B **8** (1994) 943.
26) Y. Asada, K. Slevin, and T. Ohtsuki: Phys. Rev. Lett. **89** (2002) 256601.
27) A. Kyrala: *Theoretical Physics: Applications of Vectors, Matrices, Thensors and Quaternions* (Philadelphia, London, 1967).
28) T. Nakayama and K. Yakubo: Phys. Rep. **349** (2001) 239.
29) Details of the forced oscillator method for quaternion-real matrices will be published elsewhere.
30) A. Chhabra and R. V. Jensen: Phys. Rev. Lett. **62** (1989) 1327.